# Imaging Polymer Systems with High-Angle Annular Dark Field Scanning Transmission Electron Microscopy (HAADF−STEM)

**Joachim Loos,*[,†,‡,§] Erwan Sourty,[†,∥] Kangbo Lu,[†,§] Gijsbertus de With,[†] and Svetlana v. Bavel[†,§]**

*Laboratory of Materials and Interface Chemistry and Soft-Matter CryoTEM Research Unit and Laboratory of Polymer Technology, Eindhoven University of Technology, PO Box 513, NL-5600 MB Eindhoven, The Netherlands, Dutch Polymer Institute, Eindhoven University of Technology, PO Box 902, NL-5600 AX Eindhoven, The Netherlands, and FEI Company, Achtseweg Noord 5, Building AAE, 5600 KA Eindhoven/Acht, The Netherlands*

*Received November 26, 2008; Revised Manuscript Received February 17, 2009*

ABSTRACT: We have analyzed the nanoscale organization of various polymer systems by utilizing high-angle annular dark field scanning transmission electron microscopy (HAADF−STEM). All systems under investigation are purely carbon based; in some cases staining was used for comparison with conventional transmission electron microscopy (CTEM) imaging. For contrast creation we have applied density differences rather than differences in elemental composition of the materials. Because HAADF−STEM is an incoherent imaging technique, which provides images easy to interpret due to the lack of phase contrast, the high signal-to-noise ratio and the linearity of the signal intensity, imaging artifacts are substantially reduced and additional information on the nanoscale organization of polymer materials is obtained that is not accessible by CTEM. Exemplary, we present HAADF−STEM results form four different polymer systems—a rubber blend, a carbon black filled conductive nanocomposite, a functional blend as applied for the photoactive layer of a polymer solar cell, and semicrystalline polyethylene—and discuss critically contrast origin and the advantages of HAADF−STEM imaging for morphology characterization of polymer systems.

## Introduction

As in the field of condensed matter sciences, polymer research has made extensive use of conventional transmission electron microscopy (CTEM) ever since its invention. Polymer research focuses on materials which mainly consist of carbon and other light elements. These materials are relatively weak electron scatterers and therefore give low scattering contrast. Scattering contrast may be enhanced using an objective aperture, staining, and/or low acceleration voltages, whereas phase contrast is enhanced via defocusing. These methods, however, influence the structural organization of the specimen, introduce artifacts, limit the resolution of its projected image, and make the image difficult to interpret.

In contrast, scanning transmission electron microscopy (STEM) as an incoherent imaging technique[1] only is rarely applied for the investigation of polymer materials mainly because it is meant to be a technique that shows imaging contrast mainly because of atomic number $Z$ variations of the elements in the sample under investigation. It should be mentioned that the first STEM conceived, designed, and implemented in the late sixties by Crewe and his co-workers was specifically aimed at biological applications.[2] Because polymers mainly consist of carbon and other light elements, and because the total scattering elastic cross-section varies roughly as $Z^{3/2}$, STEM imaging is mainly performed on filled or stained systems, where the contrast is created by the $Z$-variations between the filler or staining agent and the polymer matrix, or in case of polymeric multi phase systems, in which an element with higher $Z$ in the polymer chains substantially contributes to the contrast formation, e.g. the Si in PDMS[3−5] or sulfure in ionomers.[6]

However, STEM offers several advantages for the investigation of polymer materials when compared with CTEM. It provides images easy to interpret due to the lack of phase contrast, shows linearity of the signal intensity with thickness variations and has a high signal-to-noise ratio, in particular when a high-angle annular dark field (HAADF) detector is applied that is capable of single-electron counting.[7,8]

In the present study we like to demonstrate the benefit of HAADF−STEM for investigation of polymer systems that are purely carbon-based without any elements having higher $Z$ value. Briefly, the technique and contrast mechanism will be described and illustrated with application to few polymer systems.

## Experimental Section

The thermoplastic vulcanizate (TPV) was kindly provided by DSM (The Netherlands) and consist of the elastomeric phase imbedded in an isotactic polypropylene (iPP) matrix. The rubber phase has a density of 0.86 kg/m$^3$ and the iPP has a density of 0.9 kg/m$^3$, respectively.

The conductive nanocomposite sample was kindly provided by The Dow Chemical Company. It consists of a polyethylene/polyacryl matrix material (density of 0.92 kg/m$^3$) and is filled with carbon black (CB) nanoparticles (density of 1.85 kg/m$^3$).

Both, the TPV and the nanocomposite samples were sectioned at cryogenic temperature using a cryo ultramicrotome (Reichert-Jung Ultracut E). Subsequently, the thin sections were transferred on a copper TEM grid. Some TPV specimens were stained by applying common $RuO_4$ treatments.

Details on the preparation of the functional polymer blends for polymer solar cell applications can be found elsewhere.[9] Briefly, the $C_{60}$ derivative 1-(3-methoxycarbonyl)propyl-1-phenyl-[6,6]-methanofullerene (PCBM) is blended with poly[2-methoxy-5-(3′,7′-dimethyloctyloxy)-1,4-phenylenevinylene] (MDMO-PPV) and spin coated from solution on a water soluble substrate deposited on glass. Subsequently, the formed film is floated on water and transferred on the copper TEM grid.

* Corresponding author. E-mail: j.loos@tue.nl.
† Laboratory of Materials and Interface Chemistry and Soft-Matter CryoTEM Research Unit, Eindhoven University of Technology.
‡ Laboratory of Polymer Technology, Eindhoven University of Technology.
§ Dutch Polymer Institute, Eindhoven University of Technology.
∥ FEI Company.

10.1021/ma8026589 CCC: $40.75 
Published on Web 03/10/2009

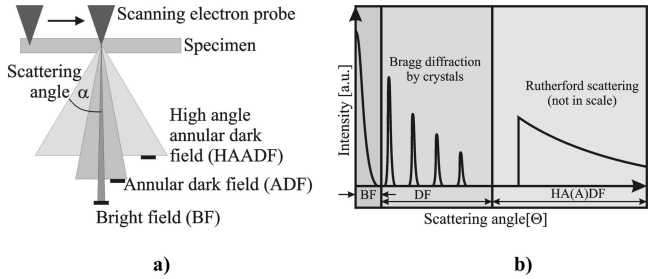


**Figure 1.** (a) Ray diagram indicating the scanning probe, the scattering angles and the respective detectors collecting the scattered electrons. (b) Qualitative representation of bright field and dark field scattering ranges (for same scattering angle ranges, the same gray scales are used for better visualization).

Finally, the high density polyethylene (HDPE) specimen was prepared by casting 0.1 wt % HDPE dissolved in xylene on hot glycerine and subsequently transferring the formed film on a copper TEM grid.

The HAADF−STEM and CTEM experiments here presented were performed on a Titan 80−300 (FEI Company, The Netherlands) equipped with a Fischione HAADF detector. The HAADF detector's "black level" was adjusted by blanking the beam (so that no electron hits the detector) then adjusting the detector offset such that the signal was just a few counts above zero (negligible compared to the detector dynamic range digitized to 16 bits). The detector gain was adjusted after unblanking the beam and making sure all levels of intensity within the scanned image were within the dynamic range of the detector.

The collection angle of the HAADF detector—fitted to the Titan 80−300 microscope used in this work—can be calculated as follows:

$$\beta_{min}[\text{rad}] = 2/(0.276 \times \text{CL}) \quad \text{and}$$
$$\beta_{max}[\text{rad}] = 10/(0.276 \times \text{CL}); \beta_{max} \leq 0.29 \text{ rad}$$

For example, a camera length CL = 100 mm the HAADF detector is able to detect scattered electrons from 72 to 290 mrad.

For the STEM imaging typical electron doses of $10^7$ electrons/nm$^2$ were applied; only for the investigation of the PE specimen was a lower dose on the order of $10^6$ electrons/nm$^2$ used.

## Results and Discussion

In CTEM, the electron beam is spread over the specimen and the transmitted beam (modulated by scattering or phase shifts within the specimen) is projected on a fluorescent screen for observation or a CCD camera or photographic emulsion for recording. Bright field (BF) CTEM images are obtained by blocking most scattered electrons (with an objective aperture) thereby enhancing the scattering contrast: dark areas have more scattering strength e.g. due to increased density or thickness than bright areas, the brightest intensity being obtained outside of the specimen (vacuum) therefore the designation "bright field".

In STEM a focused electron beam is scanned across the specimen and typically forms a probe in the range of a few nanometers or less in size. The transmitted electrons can be collected by various detectors positioned below the specimen (Figure 1a). The signal collected at the detectors is displayed on a monitor at a coordinate synchronized to the position of the beam on the specimen, giving rise to an intensity map. This is commonly referred to as a STEM image, which represents the local electron beam/specimen interaction strength, and thus provides a snapshot of the structural organization of the matter probed. Depending on the local beam-specimen interaction strength transmitted electrons are scattered at different angles. If the scattering angle is close to zero degrees the transmitted electrons can be collected by a bright field detector and the resulting image somehow has characteristics comparable to a BF CTEM image; however, STEM is operated for in-focus conditions so that less imaging artifacts are created and image interpretation is straightforward. Moreover, since in STEM the resolution is determined at the illumination side (that is before the specimen) where electrons have an energy spread below 1 eV, chromatic aberration has much less effect on resolution compared to CTEM. In CTEM the resolution is significantly altered at the imaging side (that is after the specimen) where some electrons may have lost energy up to a few thousands eV through interaction with the specimen: these electrons are focused differently by the objective lens due to chromatic aberration, resulting in a blurring of the micrograph and loss of resolution.

By using a STEM detector which only collects electrons scattered above a certain angle by the specimen, one can form a dark field (DF) STEM image whose characteristics present many advantages over BF CTEM images. In DF STEM, the minimum collection angle can be increased, so that the ratio of elastic scattered electrons (electrons scattered without loss of energy) to inelastic scattered electrons (electrons scattered with loss of energy) increases, while coherence decreases. The effects of Bragg diffraction on coherent electrons can thus be minimized.[7] For collection of electrons scattered with intermediate angle an annular dark field (ADF) detector is used, whereas a high-angle annular dark field (HAADF) detector is applied to collect the scattered electron with the largest scattering angles. Electrons with large scattering angle originate from Rutherford scattering (screened by the atoms' electronic cloud) and have the apparent advantage that contrast formation is based on elastically scattered electrons and is incoherent (Figure 1b). Besides the electron beam-specimen interaction strength the chosen *camera length* determines the collection angle, or in other words which scattered electrons are reaching the respective detectors. In a modern TEM the camera length can be varied from tens of millimeters to several meters and hence the minimum collection angle at the HAADF detector can be varied from about 200 to 2 mrad, respectively. Therefore the properties of electrons hitting the detector changes and thus the obtained image contrast can easily be optimized by adjusting the camera length. For more information on STEM the interested reader could read reference.[10]

As mentioned in the introduction the scattering elastic cross-section at large angles, varies roughly as $Z^{3/2}$. However, looking more carefully to the equation that describes the scattered to incident intensity ratio or the dark-field intensity,[11]

$$I/I_0 = 1 - e^{-N\sigma\rho t} \sim N\sigma\rho t \quad \text{for } N\sigma\rho t << 1 \qquad (1)$$

where $N = N_0/A$ is Avogadro's constant divided by the atomic weight, $\sigma$ the scattering cross section, $\rho$ the density, and $t$ the thickness of the specimen, it is evident that variations in density may result in contrast between two different polymer materials.

Figure 2 shows images of a commercial thermoplastic vulcanizate (TPV), which mainly consist of the elastomeric phase imbedded in the isotactic polypropylene matrix material. The first image is acquired in BF CTEM on an unstained specimen (Figure 2a). Some rubber domains can be identified, however, contrast between the rubber and the iPP matrix is very weak and somehow blurred; no sharp interfaces between the two phases can be identified. The dark sheet-like objects are mineral fillers. After staining, a similar specimen shows apparent contrast between the two phases (Figure 2b). Because of the higher staining efficiency of the rubber for $RuO_4$, the rubber phase appears darker within the bright iPP matrix. While the small rubber domains are homogeneous in contrast the larger domains show some gray scale variations. This might be a hint

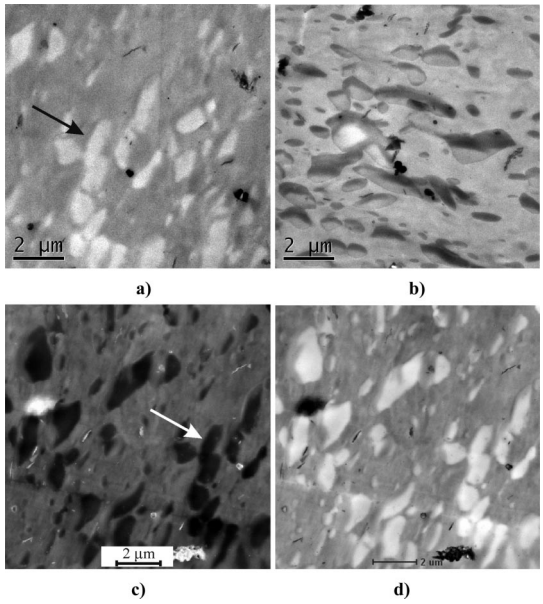


**Figure 2.** TEM images of a thermoplastic vulcanized (TPV) specimen imaged in different modes: bright field conventional TEM of (a) unstained and (b) $RuO_4$ stained specimens; (c) high-angle annular dark field scanning TEM image of the same area as imaged in 1a (arrows indicate same specimen features); (d) same image as part c but with inverted contrast.

that the composition of the rubber phase is heterogeneous with material in the center of the domains that is stained less efficiently. On the other hand, this observation might be caused also by a staining artifact, and will be discussed later in more detail.

Figure 2c represents an image of an area identical to that of the unstained specimen shown in Figure 2a; however, after applying HAADF−STEM for the visualization of the morphology. The arrows in parts a and c of Figure 2 mark the same specimen feature; the same rubber domain embedded in the iPP matrix can easily be identified. For the chosen imaging conditions the origin for contrast formation in the STEM image are the differences in the scattering intensity of the two phases. Because we are now discussing a dark field image the contrast of the polymer phases is inverted; the iPP appears bright while the rubber phase is dark. For better interpretation of the imaging result obtained by HAADF−STEM and comparison with the CTEM image of the stained specimen, Figure 1d represents the same image as Figure 2c but with different contrast adjustments and inverted contrast. The interfaces between the two phases are as clear as in case of the stained specimen and similar heterogeneity of the rubber domain appearance at the domain interface can be found. Because of the incoherent nature of HAADF−STEM imaging we can easier interpret the contrast variations in Figure 2c,d. It seems that the gray values

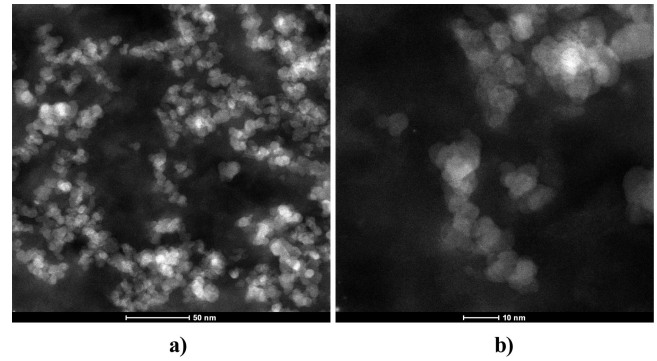


**Figure 4.** HAADF−STEM images of a conductive CB/polymer nanocomposite specimen acquired at (a) low and (b) high magnification in HAADF−STEM mode with a camera length of 200 mm.

monotonically change at the interface of the rubber domain; i.e., in HAADF−STEM this is an indication for monotonic change of the thickness of the feature under investigation. In the present case, such contrast is explained by inclination of the interface with respect to the electron beam. Certainly, because the specimen under investigation represents a section of a bulk samples, the interfaces between the rubber domains and the iPP matrix have all possible volume orientations with respect to the electron beam. However, such inclination hardly is seen in the stained specimen because staining creates an interphase with certain thickness rather than a sharp and well defined interface in the two-dimensional TEM projection of the three-dimensional specimen. Saying this, the darker parts of the rubber phases of the stained specimen (Figure 2b) represent the interfaces between the two components when viewing from a certain inclination angle, with respect to the electron beam.

We would like to note that the density difference between the rubber phase and the iPP we have applied for contrast creation is 0.04 g/cm$^3$. Qualitative discussion of the contrast mechanisms involved can be found elsewhere.[12]

In another two examples we focus on functional polymer systems, in particular on a carbon black (CB) filled conductive polymer nanocomposite and on a blend of the semiconductive polymer MDMO-PPV blended with the modified fullerenes PCBM. In both systems we are dealing with purely carbon-based fillers dispersed in a polymer matrix.

CB filled conductive nanocomposites are of particular interest, because understanding of structure−property relations of such "smart" nanocomposite materials is currently a research objective of outmost importance,[13,14] mainly focused on specific electrical and mechanical properties. Figures 3 and 4 show images of such nanocomposite material acquired in BF CTEM (Figure 3) and HAADF−STEM (Figure 4). For BF CTEM we are able to identify the CB particles when imaging the specimen in focus but contrast is low (Figure 3a); however, the interfaces between the CB fillers and the polymer matrix appear fuzzy.

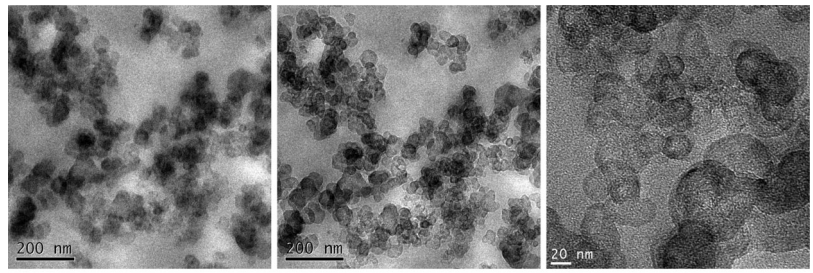


**Figure 3.** BF CTEM images of a conductive CB/polymer nanocomposite specimen acquired for (a) in-focus and (b) −5 $\mu$m defocus conditions and (c) for −1 $\mu$m defocus condition at higher magnification.

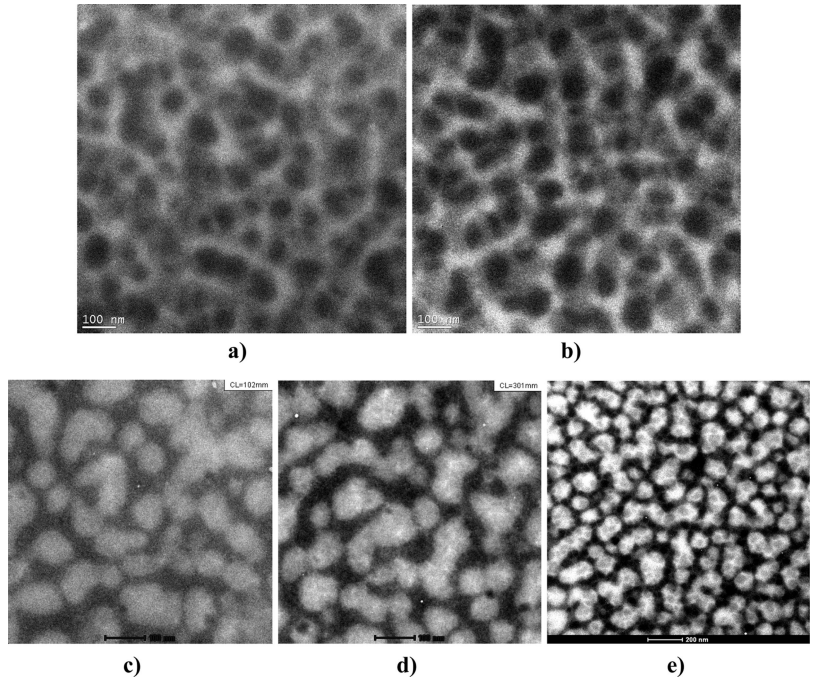


**Figure 5.** BF CTEM images of the PCBM/MDMO-PPV photoactive layer acquired at (a) 300 kV and (b) 80 kV acceleration voltage; and HAADF−STEM images of the same sample acquired with camera lengths of (c) 100 mm and (d) 300 mm, that is collection angles ranging between 73 and 290 mrad and 24 and 120 mrad, respectively. (e) Contrast optimized HAADF−STEM image showing the interconnected network of the PCBM domains.

When operating the BF CTEM in defocus conditions[15] we are able to increase the contrast between the CB and the surrounding matrix (Figure 3b), which allows for ease indentifying individual as well as aggregated CB particles because of their darker appearance in contrast with the brighter polymer matrix. When applying defocus conditions to increase the contrast we modify the phase contrast transfer function (CTF) of the TEM imaging system such that local variations of the density in our specimen, i.e., local variations of the electron density, cause phase contrast. However, we loose resolution because high spatial frequencies do not contribute anymore in an interpretable way to the image formation. In summary, defocusing in BF CTEM results in increased contrast between the CB and the surrounding matrix but causes artifact and reduces the achievable resolution. A detailed discussion on various aspects related to the CTF can be found in reference.[10]

Figure 3c shows a higher magnification image of the same specimen. We clearly identify Fresnel fringes around the CB particles, which may blow up the size of the particles, and we see an overall granularity that is present in the whole image. For this higher magnification still we are able to recognize the CB particles because of the sensitivity of our human eyes; however, the interfaces between CB and the surrounding matrix are blurred and smeared out so that, e.g., automatic detection of the CB particles with help of image processing routines is a challenge.

Figure 4 shows images of the same CB filled polymer nanocomposite specimen acquired by HAADF−STEM. For the chosen imaging conditions (200 mm camera length) contrast is formed because of different Rutherford scattering intensities of the CB and the surrounding matrix; however, for longer camera lengths diffraction contrast significantly will contribute to image formation (see discussion below on the PCBM/MDMO-PPV system). Because of their higher inelastic scattering cross section in the HAADF−STEM images the CB particles appear bright in the dark polymer matrix. Without difficulty we can identify the individual CB particles and their clusters (Figure 4a). In contrast with the high-resolution BF CTEM image (Figure 3c), in which the CB particles appear fuzzy and show a granular structure the high-magnification HAADF−STEM image shows clear and sharp interfaces between the CB particles and the polymer matrix (Figure 4b). In the case of HAADF−STEM we are able e.g. to define an intensity threshold straightforward to distinguish between the CB particles and the polymer matrix, which is very beneficial for automated image processing, especially when performing electron tomography for reconstruction of the volume organization of the specimen under investigation.

A somewhat similar functional polymer system is PCBM/MDMO-PPV, which is used as photoactive layer in polymer solar cells.[16,17] Such a layer is the so-called bulk heterojunction, in which the two components phase separate and, in the ideal case, form a nanoscale cocontinuous network that guarantees efficient charge separation at interfaces and carrier transport from any location within the layer to the two corresponding electrodes. Figure 5 shows images of the morphology of a photoactive layer acquired for defocus conditions by BF CTEM at two different acceleration voltages, at 300 kV and at 80 kV, respectively. The image acquired at high acceleration voltage has only weak contrast between the PCBM domains (dark areas) and the surrounding MDMO-PPV matrix (Figure 5a). A standard approach in polymer sciences for increasing contrast in BF CTEM is to lower the acceleration voltage, which increases the actual interaction cross-section of the electrons with the specimen under investigation. Figure 5b represents the morphology of a similar specimen area as shown in Figure 5a but acquired at the acceleration voltage of 80 kV. Now, we can distinguish the PCBM domains from the MDMO-PPV matrix polymer; the contrast between the two components indeed has increased. The average PCBM domain size is about 100 nm and some of the domains seem to be connected with each other. However, the image has a distinct granular appearance (as for the CB system for similar imaging conditions, Figure 3b,c) and the interfaces between the PCBM domains and the matrix are fairly fuzzy so that edges of the PCBM domains hardly can be identified. Parts c and d of Figure 5 show HAADF−STEM

images acquired on the same specimen but with two different camera lengths and collection angle-ranges at the HAADF detector. Because of its higher density the PCBM appears bright and the surrounding MDMO-PPV matrix is dark when imaging in dark field conditions.

When monitoring a specimen in HAADF−STEM mode, low camera lengths (i.e., large collection angles) exclude contributions from diffraction contrast possibly originating from a (semi-) crystalline sample whereas for longer camera lengths (i.e., lower collection angles) a substantial part of the image contrast is a result of the diffraction signal. For a short camera length (i.e., large collection angles) good contrast between the PCBM domains and the matrix exist (Figure 5c). Contrast and appearance between the two components is somewhat similar with the BF CTEM image acquired at low acceleration voltage; however, the PCBM domains show distinct contrast with the MDMO-PPV matrix.

Applying a longer camera length (i.e., lower collection angles) but otherwise similar imaging conditions, the contrast between the PCBM domains and the MDMO-PPV matrix substantially increases (Figure 4d). Because PCBM forms nanocrystals when prepared as in the present case,[18] in the HAADF−STEM image additional diffraction contrast contributes to the image formation. Because of higher contrast, high signal-to-noise ratio and imaging for in-focus conditions the image appears less blurred and we can see clear interfaces between the PCBM domains and the surrounding MDMO-PPV matrix. Most of the domains are connected with each other and form aggregates. Only few PCBM domains are isolated and both the PCBM as well as the MDMO-PPV form interpenetrating networks throughout the whole photoactive layer.

When inspecting carefully the HAADF−STEM image obtained at long camera length we can recognize even more morphological details, which were not visible in the previously discussed imaging modes. Beside the dominant PCBM domains, tiny PCBM nanobridges are seen that are crossing the MDMO-PPV matrix and connect the domains with each other. These nanobridges create additional interface in the photoactive film for effective exciton dissipation and a fine dispersed network for charge transport to the respective electrode.

Finally, we would like to discuss results obtained on semicrystalline polyethylene. In general, electron microscopy of polymer materials is a delicate task mainly because of the beam sensitive nature of these materials. Therefore, one key issue toward reliable TEM data is controlling the electron dose to prevent beam damage of the specimen. This is in particular valid when we investigate semicrystalline or other polymers, which already for low electron doses change their macromolecular organization or degrade. In this respect, STEM is meant to be a high electron dose technique because it applies a highly focused and thus high intensive electron probe moving across the specimen. However, because modern HAADF detectors have high sensitivity and can detect single electrons, the scanning rate and beam intensity can be adjusted accordingly to reduce the actual dose exposed to the specimen.

We have prepared a thin solution cast film of HDPE and investigated its morphology by HAADF−STEM imaging. Of course, characterization of such a specimen easily can be performed by BF CTEM for phase contrast imaging conditions; however, our intention is to demonstrate with a well-known specimen that imaging of such electron beam sensitive semicrystalline HDPE is possible in HAADF−STEM mode. We would like to note that already in the late 1970s Khoury and a co-worker have shown that ADF−STEM successfully can be applied to reveal information on the organization of solution grown PE single crystals by utilizing diffraction contrast.[19]

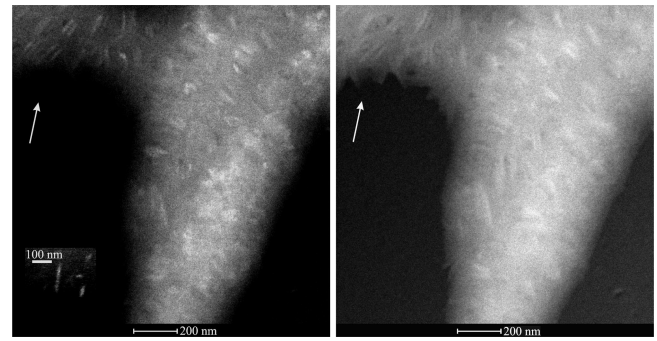


**Figure 6.** Two subsequently acquired HAADF−STEM images of the same HDPE specimen area: (a) first acquisition showing diffraction contrast of lamellae which is most clear at the position indicated by the arrow (see also inset) and (b) second acquisition showing only diffuse thickness contrast.

After careful adjusting the imaging conditions including the electron dose applied (~60 electrons/nm$^2$/s), the HAADF−STEM of the thin HDPE film specimen shows few lamellar crystals (Figure 6a). Because of their higher density when compared with the amorphous phase and their crystalline state, which provides diffraction contrast for a long camera length of 300 mm, the HDPE crystals appear bright in the STEM image. When imaging the same area a second time (Figure 6b) the contrast of the HDPE crystals has been vanished, which indicates that the crystals are destroyed. However, because of cross-linking and some thickness contrast still the lamellae are somewhat visible but blurred.

## Conclusions

In our study, we have demonstrated the versatility of HAADF−STEM for the morphological characterization of polymer systems with high resolution. All the investigated systems purely consist of carbon or lighter elements and no additional staining with heavy elements like ruthenium or osmium needs to be performed. For all systems local variations of the density can be utilized to create HAADF−STEM images with high contrast and high signal-to-noise ratio. In case of the rubber system, we easily can distinguish between the two phases and gain additional information on the interface organization, which is somewhat hidden when applying staining procedures. Moreover, staining may generate artifacts and is, at least, an additional preparation step which is time-consuming and can be skipped by applying HAADF−STEM.

For both carbon nanoparticle filled systems discussed, HAADF−STEM is able to create excellent contrast between the components. Because imaged in focus the CB/polymer interface appears very clear and not blurred as in the case when applying BF CTEM, which is very helpful, e.g., for reliable quantification of the images obtained. For the PCBM/MDMO-PPV system, we are able to visualize beside the dominant PCBM domains a fine network of PCBM nanowires by increasing the camera length and thus utilizing additional diffraction contrast. Finally, by careful adjustment of the imaging conditions, we have demonstrated that we can image the highly electron beam sensitive lamellar crystals of HDPE.

On the basis of the results presented, we believe that HAADF−STEM is a very powerful tool for high resolution imaging of unstained polymer systems, in general.

**Acknowledgment.** The authors would like to thank Ralph Guerra (The Dow Chemical Company, Midland, MI), Georg Bar (Dow Olefinverbund GmbH, Germany) and Bob Vastenhout (Dow Benelux B.V., The Netherlands) for technical assistance by preparing the polymer nanocomposite specimens filled with carbon black

nanoparticles, and Martin van Duin (DSM Research) and Rudy Debliek (DSM Resolve) for assistance by preparing the rubber specimens. The work forms part of the Dutch Polymer Institute (DPI) research program. Additional financial support was provided by the Dutch Science Organization (NWO).

## References and Notes

(1) Nellist, P. D.; Pennycook, S. J. *Ultramicroscopy* **1999**, *78*, 111.
(2) Crewe, A. V.; Wall, J. *J. Mol. Biol.* **1970**, *48*, 375.
(3) Drummy, L. F.; Wang, Y. C.; Schoenmakers, R.; May, K.; Jackson, M.; Koerner, H.; Farmer, B. L.; Mauryama, B.; Vaia, R. A. *Macromolecules* **2008**, *41*, 2135.
(4) Kim, G.; Sousa, A.; Meyers, D.; Libera, M. *Microsc. Microanal.* **2008**, *14*, 459.
(5) Benetatos, N. M.; Chan, C. D.; Winey, K. I. *Macromolecules* **2007**, *40*, 1081.
(6) Zhou, N. C.; Chan, C. D.; Winey, K. I. *Macromolecules* **2008**, *41*, 6134.
(7) Clarke, D. R. *J. Mat. Sci.* **1970**, *5*, 689.
(8) Crewe, A. V. *J. Ultrastruct. Res.* **1984**, *88*, 94.
(9) Yang, X.; van Duren, J. K. J.; Janssen, R. A. J.; Michels, M. A. J.; Loos, J. *Macromolecules* **2004**, *37*, 2151.
(10) Reimer, L. and Kohl, H., *Transmission Electron Microscopy: Physics of Image Formation*, 5th ed.; Springer-Verlag, New York, 2008; p 188.
(11) Heidenreich, R. D. *Fundamentals of Transmission Electron Microscopy*; Wiley: New York, 1964; p 31.
(12) Sourty, E.; van Bavel, S.; Lu, K.; Guerra, R.; Bar, G.; Loos, J. *Microsc. Microanal.*, in press.
(13) Sichel, E. K. *In Carbon black-polymer composites*, Marcel Dekker, New York, 1982.
(14) Dai, K.; Xu, X.-B.; Li, Z.-M. *Polymer* **2007**, *48*, 849.
(15) Miles, M.; Petermann, J. *J. Macromol. Sci., Phys.* **1979**, *B16*, 1.
(16) Hoppe, H.; Sariciftci, N. S. *J. Mat. Chem.* **2006**, *16*, 45.
(17) Yang, X.; Loos, J. *Macromolocules* **2007**, *40*, 1353.
(18) Yang, X.; van Duren, J. K. J.; Rispens, M. T.; Hummelen, J. C.; Janssen, R. A. J.; Michels, M. A. J.; Loos, J. *Adv. Mater.* **2004**, *16*, 802.
(19) Khoury, F.; Bolz, L. H. *38th Annual Proceedings, Electron Microscopy Society of America*; Electron Microscopy Society of America: Woods Hole, MA, 1980; pp 242−245.

MA8026589